J. Fluid Mech. (2008), *vol.* 600, *pp.* 181–199.
doi:10.1017/S0022112008000487 Printed in the United Kingdom

Temporal variation of non-ideal plumes with sudden reductions in buoyancy flux

M. M. SCASE[1]†, C. P. CAULFIELD[2,1] AND S. B. DALZIEL[1]

[1]Department of Applied Mathematics and Theoretical Physics, University of Cambridge, Centre for Mathematical Sciences, Wilberforce Road, Cambridge CB3 0WA, UK

[2]BP Institute, University of Cambridge, Madingley Road, Cambridge CB3 0EZ, UK

(Received 20 February 2007 and in revised form 18 December 2007)

We model the behaviour of isolated sources of finite radius and volume flux which experience a sudden drop in buoyancy flux, generalizing the previous theory presented in Scase *et al.* (*J. Fluid Mech.*, vol. 563, 2006, p. 443). In particular, we consider the problem of the source of an established plume suddenly increasing in area to provide a much wider plume source. Our calculations predict that, while our model remains applicable, the plume never fully pinches off into individual rising thermals.

We report the results of a large number of experiments, which provide an ensemble to compare to theoretical predictions. We find that provided the source conditions are weakened in such a way that the well-known entrainment assumption remains valid, the established plume is not observed to pinch off into individual thermals. Further, not only is pinch-off not observed in the ensemble of experiments, it cannot be observed in any of the individual experiments. We consider both the temporal evolution of the plume profile and a concentration of passive tracer, and show that our model predictions compare well with our experimental observations.

1. Introduction

Turbulent plumes and jets arise in a wide range of geophysical and industrial contexts. Recently (Scase *et al.* 2006*b*, herein referred to as S06*b*) we developed a generalized time-dependent model (based on the famous Morton, Taylor & Turner 1956 model) to consider such flows. It was predicted that, whilst the model remained valid, plumes could not be made to separate into individual thermals by a reduction in the driving-source strength. The developed time-dependent model was found to support a separable power-law solution which is realized when the driving-source strength of the plume or jet is significantly reduced. This separable power-law solution predicts a narrowing of the plume radius, but not total pinch-off, and the solution is closely related to a solution originally presented by Batchelor (1954) as a model for convective plumes in an unstably stratified ambient fluid. The flow may be considered to consist of three regions. Far from the source, the plume behaves as a classical plume with the original source buoyancy flux. Conversely, near the source, the plume behaves as a classical plume with the final, new, source buoyancy flux. The plume approaches the separable power-law solution in the intermediate region connecting

† Present address: 128 Upson Hall, Sibley School of Mechanical and Aerospace Engineering and Department of Mathematics, Cornell University, Ithaca, NY 14853, USA.

these two classical plume structures. In this paper, we present experimental verification of this core prediction.

The solutions to the time-dependent model presented in S06*b* and Scase, Caulfield & Dalziel (2006*a*) (herein referred to as S06*a*) concentrated on point-source plumes in pure plume balance in unstratified and stratified background fluids, respectively. We demonstrate in the present paper that in fact neither of these constraints (that the plume has a point source, or the plume is in pure plume balance), is essential for realizing the separable solutions found in S06*b* for an unstratified background fluid. It is the reduction in source strength which is the key requirement of the model. We investigate briefly a case with relevance to geophysical and industrial applications in which the size of the source of the plume expands catastrophically at some time. Examples of when such behaviour might be expected include volcanic eruptions and devastating releases of toxic buoyant jets at industrial plants. We find again that, provided this expansion of the source results in a weaker buoyancy flux, the separable solutions identified in S06*b* are realized, and the general behaviour remains.

We present here experiments that are complementary to the theory developed in S06*b*. We conducted a total of 100 nominally identical experiments to provide an ensemble for comparison with the theory and we found good agreement. In previous experimental studies of plumes with statistically steady source conditions (as recently collated and compared in Carazzo, Kaminski & Tait 2006) a simple time average of the experiment can typically be used as the 'ensemble' of the turbulent plume. In the present study, due to the time-dependent nature of the source conditions, a true ensemble over separate realizations of nominally identical experiments must be used. This, allied with the inherent time dependence of the flow, introduces some extra practical difficulties compared to previous studies. Methods for dealing with these difficulties, in particular the synchronization of the individual experiments, are discussed later in § 4.

The layout of the present paper is as follows. In § 2 we establish the mathematical notation used to describe the problem. The notation is similar to that used in S06*b*, S06*a* and Scase *et al.* (2006*c*, 2007). In § 3 we investigate the problem of non-ideal plumes that undergo rapid reductions in their source strength in preparation for comparison with experiment. We also consider variations in source radius, which are of course possible when the source has non-zero volume flux (we define non-ideal plumes as plumes with non-zero source volume flux). In § 4 we discuss the experimental arrangement used and then in § 5 we conduct an analysis of our results. Finally in § 6 we draw our conclusions.

2. Theoretical nomenclature

As in S06*b* and S06*a* we assume a top-hat distribution of both density and vertical velocity throughout our theoretical modelling. Throughout we denote dimensional quantities as $\cdot_\star$ where $\cdot$ denotes the corresponding non-dimensional quantity.

The density of the plume fluid is a function of both space and time and is denoted $\rho_\star(z_\star, t_\star)$. We assume that the ambient fluid is unstratified, and so its density is a constant, denoted by $\rho_{\infty\star}$. The vertical velocity of the plume and the plume radius, like the density, are functions of both space and time and are denoted $w_\star(z_\star, t_\star)$ and $b_\star(z_\star, t_\star)$, respectively.

Following Morton *et al.* (1956), we define a true mass flux, true momentum flux and true buoyancy flux, respectively, as

$$Q_\star = \int_0^{2\pi}\int_0^{\infty} w_\star \rho_\star \, r_\star \mathrm{d}r_\star \mathrm{d}\theta = \pi b_\star^2 w_\star \rho_\star, \tag{2.1a}$$

$$M_\star = \int_0^{2\pi}\int_0^{\infty} w_\star^2 \rho_\star \, r_\star \mathrm{d}r_\star \mathrm{d}\theta = \pi b_\star^2 w_\star^2 \rho_\star, \tag{2.1b}$$

$$F_\star = \int_0^{2\pi}\int_0^{\infty} w_\star g_\star \left(\rho_{\infty\star} - \rho_\star\right) r_\star \mathrm{d}r_\star \mathrm{d}\theta = \pi b_\star^2 w_\star g_\star \left(\rho_{\infty\star} - \rho_\star\right), \tag{2.1c}$$

where $g_\star$ is the acceleration due to gravity. There is a factor of π difference between the present definitions of $Q_\star$, $M_\star$ and $F_\star$ and those used in S06*b* and S06*a*. This factor has been introduced to avoid confusion with directly measured experimental fluxes in the present paper. We make the Boussinesq approximation and assume the standard entrainment assumption of Morton *et al.* (1956) such that $u_{e\star} = -\alpha w_\star$, where $u_{e\star}$ is the (horizontal) velocity of the ambient fluid being entrained into the plume at the plume boundary (see figure 1 of S06*b*). Note that we make the simplifying assumption that we may use a constant value of α, meaning that we assume the value of α is the same whether we are considering a plume or a jet, or something in between. Although a constant α is thought not to be exactly true in practice (see Kaminski, Tait & Carazzo 2005 for a full discussion), we believe that this simplifying assumption does not change the fundamental aspects of the time-dependent system considered here.

We introduce the following non-dimensional quantities based on an arbitrary dimensional length scale $z_{\ell\star}$, such that $z_\star = z_{\ell\star} z$, and the buoyancy flux scale $F_{0\star}$, such that

$$Q_\star = (4\alpha^2\pi\rho_{\infty\star})^{2/3} F_{0\star}^{1/3} z_{\ell\star}^{5/3} Q, \quad M_\star = (4\alpha^2\pi\rho_{\infty\star})^{1/3} F_{0\star}^{2/3} z_{\ell\star}^{4/3} M, \tag{2.2a,b}$$

$$F_\star = F_{0\star} F, \quad t_\star = \left(4\alpha^2\pi\rho_{\infty\star}\right)^{1/3} F_{0\star}^{-1/3} z_{\ell\star}^{4/3} t. \tag{2.2c,d}$$

Non-dimensional and dimensional plume radius, plume velocity and reduced gravity can be expressed in terms of the non-dimensional bulk fluxes as

$$b = \frac{b_\star}{2\alpha z_{\ell\star}} = \frac{Q}{M^{1/2}}, \tag{2.3a}$$

$$w = \left\{\frac{4\alpha^2\pi\rho_{\infty\star}}{F_{0\star}}\right\}^{1/3} z_{\ell\star}^{1/3} w_\star = \frac{M}{Q}, \tag{2.3b}$$

$$g' = \left\{\frac{4\alpha^2\pi\rho_{\infty\star}}{F_{0\star}}\right\}^{2/3} z_{\ell\star}^{5/3} g'_\star = \frac{F}{Q}. \tag{2.3c}$$

Under this non-dimensionalization, the system of equations governing the spatio-temporal evolution of a plume in an unstratified ambient background fluid is given by (S06*b*)

$$\frac{\partial}{\partial t}\left(\frac{Q^2}{M}\right) + \frac{\partial Q}{\partial z} = M^{1/2}, \tag{2.4a}$$

$$\frac{\partial Q}{\partial t} + \frac{\partial M}{\partial z} = \frac{QF}{M}, \tag{2.4b}$$

$$\frac{\partial}{\partial t}\left(\frac{QF}{M}\right) + \frac{\partial F}{\partial z} = 0. \tag{2.4c}$$

It should be noted that there is no dependence on the length scale $z_{\ell\star}$ in the system (2.4). This can be viewed as being a result of the self-similarity of the system, in particular the dependence of the time scale on the length scale $z_{\ell\star}$.

In order for a plume to be considered a 'pure' plume, the mass flux, momentum flux and buoyancy flux must be exactly balanced at all heights in the plume such that the non-dimensional quantity

$$\Gamma = \frac{5}{4}\frac{Q^2 F}{M^{5/2}}, \tag{2.5}$$

(originally defined by Morton 1959) defined in terms of the non-dimensional fluxes, is exactly equal to unity. We may expect that in any real flow there will be some deviation from this value at all finite heights and therefore the plume will not be a pure plume. These types of plumes were first considered by Morton (1959) and more recently by Caulfield (1991) and Hunt & Kaye (2001), for example. A plume originating from a physical, non-point, source (i.e. one distributed source over a finite area) typically has a deficiency of momentum compared to an ideal plume. Such a plume is referred to as 'lazy' and has $\Gamma > 1$ (cf. (2.5)). A forced plume (equivalently a buoyant jet) may have an excess of momentum compared to a pure plume and (2.5) demonstrates that such a plume has an associated value of $\Gamma < 1$. Finally, a 'point-source' plume has a source of zero radius, and hence zero source volume flux. Experimentally, if the buoyancy of the flow is caused by variations in salinity, it is necessary to have sources with non-zero volume flux (and hence radius). We refer to plumes rising from such sources as being 'non-ideal'; of course such finite-source volume flux flows are also relevant in geophysical and industrial situations.

3. Modelling for direct comparison with experiment

We attempted to conduct experiments which exactly complement the theory presented in S06*b*, specifically through maintaining pure plume balance at all times. We used two different plume-source fluids, of differing density. We were able to establish a strong steady pure plume with an initial very-buoyant fluid and then swapped the source fluid to a new lower-buoyancy fluid, whilst maintaining pure plume balance. However, due to the finite volume of the turbulent plume nozzle employed (see §4 for a description) and the very low flow rates through it, we found that the new less-buoyant fluid mixed with the old more-buoyant fluid, before entering the main experimental tank, over periods far greater than the time ($\sim$10 s) for a buoyant parcel of fluid to leave the nozzle and reach the top of the tank. So, regardless of how swiftly the source fluids were changed, the buoyancy flux at the source changed over a time scale that was too long for the expected transition in the plume to be observed. The only way to change the buoyancy flux rapidly enough, in the present arrangement, was to change the flow rate of the plume fluid, keeping its density constant, which in turn meant preserving a pure plume balance throughout the experiment was impossible. However, as shown below, this does not change the fundamental character of the flow.

3.1. *Non-ideal source conditions*

As was shown in S06*b* for an unstratified ambient fluid, there exists a separable power-law solution to (2.4) that is stable to small perturbations travelling with the local plume velocity. Numerical experiments verified that this was indeed the case for ideal plume-source conditions. However, the separable power-law solutions, specifically

(cf. S06*b*, (3.11))

$$Q = \frac{1}{18}\frac{z^3}{t}, \quad M = \frac{1}{36}\frac{z^4}{t^2}, \quad F = \frac{1}{36}\frac{z^4}{t^3}, \tag{3.1}$$

have no dependence on the boundary conditions at the source. Hence, we may expect this stable separable solution to be realized whenever the driving-source conditions of an arbitrary non-ideal plume are reduced sufficiently.

It has been established that plumes with non-ideal source conditions at large distances from their source have profiles asymptotically given by $b = 3(z+z_e)/5$ (within our non-dimensionalization), where z_e is known as the virtual origin correction (see e.g. Morton 1959, Caulfield 1991, Caulfield & Woods 1995, Hunt & Kaye 2001). At large distances, the plume appears to come from a pure plume point source situated some distance away from the actual source.

In S06*b* it was shown that when the driving fluxes of a pure point-source plume were reduced, maintaining a pure point-source plume balance throughout, there exists a finite connecting region in the plume the fluxes of which are well described by the separable solutions (3.1). However, given the need for virtual origin corrections when dealing with steady plumes with non-ideal source conditions, it might be expected that a similar virtual origin correction would be needed for the narrowing connecting region. As observed above however, since the solutions (3.1) contain no information about the source conditions, we should expect this narrowing region not to be affected by mismatches in the source conditions and therefore not require any virtual origin correction, even though the location of the source is important through the z dependence of (3.1).

Figure 1(*a*) demonstrates that the separable solutions in (3.1) require no virtual origin correction to be made when applying them to the decreasing source strength problem. The plume-source radius is fixed as $b(0, t) = 1$ throughout. The initial state of the system is taken to be a steady plume. The initial non-dimensional buoyancy flux at the source is $F(0, 0) = 1$, while the initial mass and momentum fluxes at the source are chosen to yield a forced plume with $\Gamma(0, 0) = 10^{-2}$. The initial forced plume profile is shown as a thin solid line. Since the plume is forced, its profile lies outside that of a pure plume, $b = 3z/5$, shown as a dashed line. (Within this non-dimensionalization, a steady point source of momentum alone – i.e. a pure jet – would have a profile $b = z$, assuming that the entrainment constant can be considered identical for both plumes and jets, and is therefore independent of Γ.) At $t = 0$, the source conditions are changed to new steady values so that the plume radius at the origin remains at $b(0, t) = 1$, but we make the plume lazy by increasing Γ so that $\Gamma(0, t > 0) = 10^2$, and we reduce the driving buoyancy flux so that $F(0, t > 0) = 10^{-2}$.

For $t > 0$ we have new steady lazy source conditions and so we expect the plume to establish itself as a new steady lazy plume based on the new source conditions. The lazy plume profile supported by the new source conditions is shown with a dotted line and it can be seen that at $t = 2.38$ the plume profile (shown as a thick solid line in figure 1*a*) lies on top of the anticipated new steady lazy plume profile (shown as a dotted line) near the source ($z < 0.5$). The information about the changes in source conditions has not yet fully propagated up the shown plume profile, so the upper part of the plume still lies on the initial forced plume profile plotted with a thin solid line. For $0.5 \lesssim z \lesssim 4$ we see a narrower region, connecting the upper and lower parts of the plume, which is well described by the separable solution (3.1) that predicts $b = z/3$.

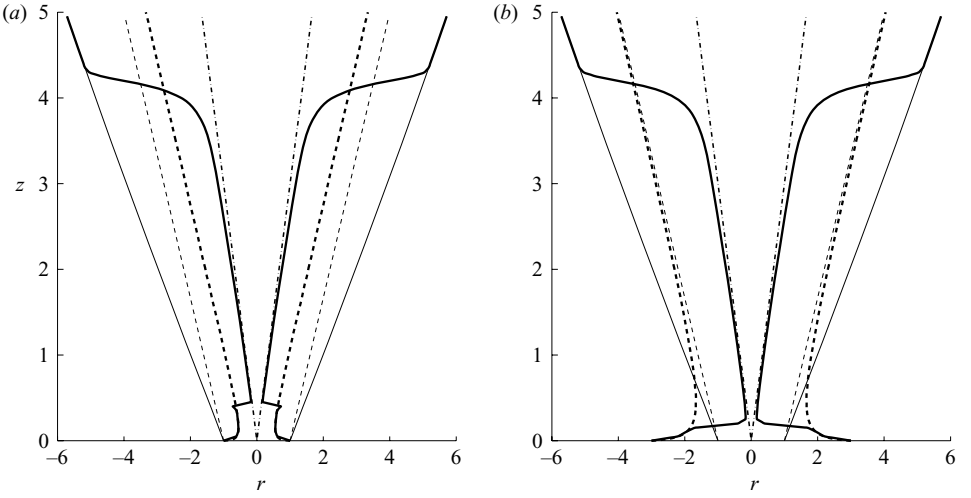

FIGURE 1. (*a*) A numerical solution of (2.4) showing the profile of the steady initial forced plume (plotted with a thin solid line), the final lazy profile (bold dashed line) and the observed plume shape at an intermediate non-dimensional time $t = 2.38$ (bold solid line). The classical steady pure-plume solution is shown with a thin dashed line and the predicted minimum width $b = z/3$ with a dot-dashed line. Initially, the plume has a laziness parameter $\Gamma = 10^{-2}$ making it strongly forced; at $t = 0$ the laziness parameter is increased to $\Gamma = 10^{2}$ making the plume very lazy. The source radius is maintained at $b(0, t) = 1$ and the buoyancy flux is reduced from $F = 1$ to $F = 10^{-2}$. (*b*) The same conditions and line types were used as for figure 1(*a*) except that for $t > 0$, the source size was increased from its initial value, $b(0, 0) = 1$, to $b(0, t) = 3$. This again shows the plume narrowing to $b = z/3$.

As can be seen, even though there has been a large mismatch in the source conditions resulting in strongly forced and strongly lazy plumes from a distributed (i.e. not a point) source, the transient connecting region still agrees closely with the separable solutions (3.1). The required virtual origin corrections for the initial forced plume and final lazy plume shown are $z_{vs} = 9.33$, and $z_{vs} = 0.57$, respectively. For comparison, a pure plume with this initial source radius would have $z_{vs} = 5/3$. (These initial and final states can be equivalently thought of as rising from distributed sources of buoyancy alone with source radius $b_{vs} = 5.60$ and $b_{vs} = 0.34$, respectively.) The requirement for a virtual origin correction is not observed in the narrow matching region. (A brief derivation of the calculation for virtual origin corrections for forced plumes with $\Gamma < 1/2$ is given in the Appendix.)

From these calculations, we see once again that it is extremely difficult to break an established plume into thermals by reductions in the source strength alone.

3.2. *The source area expansion problem*

We have established in S06*b* the required mathematical tools with which to deal with the geophysically and industrially relevant case of a plume-source area increasing, for example during a volcanic explosion or industrial accident (the case of the plume source shrinking can be treated in much the same way, but has not been considered here).

Figure 1(*b*) shows the predicted top-hat plume profile for a plume whose source area increases after the initial plume has been established. Initially, the plume has a distributed source such that $b(0, 0) = 1$. The initial buoyancy flux is $F(0, 0) = 1$, and the mass and momentum fluxes have been chosen such that $\Gamma(0, 0) = 10^{-2}$, a forced

plume, as in figure 1(*a*). For $t > 0$, the size of the source is increased from $b(0, 0) = 1$ to $b(0, t) = 3$. Simultaneously, Γ is increased from $\Gamma(0, 0) = 10^{-2}$ to $\Gamma(0, t) = 10^{2}$ changing the plume from forced to lazy, and the source buoyancy flux is reduced from $F(0, 0) = 1$ to $F(0, t) = 10^{-2}$.

The thick solid line in figure 1(*b*) shows the plume profile at a non-dimensional time $t = 2.38$ after the changes in source condition have been made. After a long time we expect the source to establish a new steady plume based on these new source conditions. This steady lazy plume profile is shown as a dotted line. It can be seen that near the source ($z < 0.2$), the plume is beginning to establish this new steady plume, since the thick solid line lies on top of the dotted line. We observe that even though the area of the source has been increased by approximately an order of magnitude, the transient connecting region of the plume still narrows and is in good agreement with the $z/3$ plume profile predicted by the separable solutions in (3.1). In particular, although very strongly narrowed, the plume does not pinch-off into individual thermals.

It should be noted here that the derivation of the system of equations (2.4), as in the steady model of Morton *et al.* (1956), required the assumption that the plume was 'thin' with the length scale of vertical changes in properties being large compared with the plume width, in order for terms involving the pressure field to be ignored. This assumption is violated in the source-rupture problem and it is not clear that it is necessarily valid for any distributed source plume (see e.g. Caulfield 1991, Caulfield & Woods 1995, Hunt & Kaye 2001) or indeed any non-Boussinesq plume (see e.g. Woods 1997). However, these models have proved useful for distributed-source lazy plumes and non-Boussinesq plumes and so we may expect predictions about such source-rupture problems to be useful, but caution should be exercised.

3.3. *Evolution of passive tracer fields*

For direct comparison with experimental measurements it is convenient to make predictions for the evolution of a passive tracer based on the model equations (2.4). We add a fourth equation to the system (2.4) for a fourth unknown, the passive tracer concentration. We define a pointwise passive tracer concentration $c_\star(r_\star, z_\star, t_\star)$ (i.e. $c_\star(r_\star, z_\star, t_\star)$ is zero for $r_\star > b_\star$ and is independent of $r_\star$ for $r_\star < b_\star$; as before, stars denote dimensional quantities) and define a pointwise non-dimensional passive tracer concentration such that $c_\star = c_{0\star} c$, where $c_{0\star}$ is a reference concentration, taken to be the passive tracer concentration within the plume at $z_\star = 0$, $t_\star = 0$. In the absence of any tracer in the ambient fluid, the evolution equation for the passive tracer is given dimensionally by

$$\frac{\partial c_\star}{\partial t_\star} + \nabla \cdot (c_\star \boldsymbol{u}_\star) = 0. \tag{3.2}$$

Following the method of derivation described in S06*b*, a pointwise non-dimensional top-hat concentration distribution satisfies

$$\frac{\partial}{\partial t}\left(\frac{Q^2 c}{M}\right) + \frac{\partial}{\partial z}(Qc) = 0; \tag{3.3}$$

note the relation to (2.4*c*) when c is replaced by $F/Q = g'$. Thus, it immediately follows that in a steady plume $c_\star/c_{0\star} = g'_\star/g'_{0\star}$. This may be expected since c indicates how diluted that initial plume fluid is with non-buoyant ambient fluid. There are two advantages to defining a separate concentration equation, however. Firstly, the concentration equation (3.3) remains valid when the ambient fluid is stratified, whereas

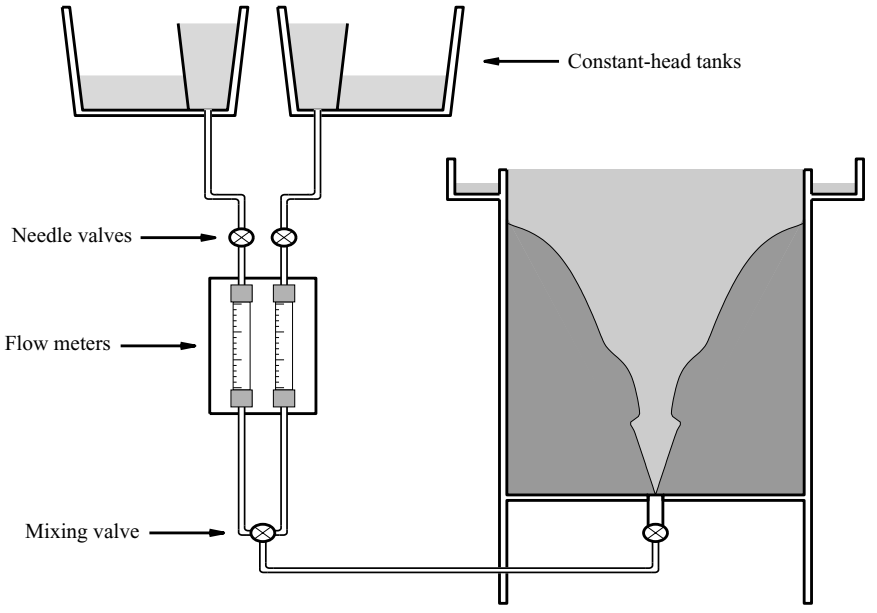

FIGURE 2. Schematic representation of the experimental set-up. Two constant head tanks containing identical fluid, (which is buoyant compared to the ambient fluid in the tank) are connected via two flow meters to a mixing valve. This mixing valve controls the flow from the two header tanks to the plume nozzle underneath the experimental tank.

the simple relationship $c \propto g'$ does not, since the right-hand side of (2.4*c*) becomes non-zero (see (2.16*c*) in S06*b*), but the right-hand side of (3.3) remains zero. Secondly, and relevantly in the present context, the concentration strength at the source, $c(0, t)$, can be kept constant, while changing the reduced gravity at the source, $g'(0, t)$. This means, experimentally, that a strong plume which is significantly weakened at a given time does not introduce a necessary large reduction in the light levels.

4. Experimental setup

4.1. *Experimental arrangement*

A schematic representation of the experimental setup used is shown in figure 2. Two identical constant-head tanks were arranged above the main experimental tank which had dimensions $0.70\,\mathrm{m} \times 0.70\,\mathrm{m} \times 1.32\,\mathrm{m}$. The constant-head tanks comprised an inner feeder section and an outer overflow section, with fluid constantly pumped from the overflow section into the feeder section at a rate faster than the rate of draining from the feeder section. This ensured that the volume of fluid in the feeder section remained approximately constant, even though fluid was being continuously drained. Each constant-head tank contained identical fluid, fresh water, which was buoyant compared to the brine used for the ambient fluid in the main experimental tank. The constant-head tanks were connected via needle valves, to control the flow rate, through two flow meters and then to a mixing valve. The needle valves were used to set the maximum flow rate of buoyant fluid from each constant head tank to the mixing valve. The mixing valve adjusted the flow rate from each constant head tank into the turbulent plume nozzle.

The plume nozzle† was designed to create a fully turbulent plume. Fluid entered the base of the nozzle through a small 'pin-hole' into an expansion chamber which triggered the turbulence transition. The turbulent fluid then passed through a constriction into the main experimental tank which contained the stationary, homogeneous ambient fluid. The main experimental tank had an overflow at the top meaning that buoyant plume fluid which reached the top of the tank could overflow, keeping the amount of fluid in the main experimental tank constant. This overflow also reduced, but did not eliminate, difficulties associated with the 'filling-box' phenomenon (Baines & Turner 1969) and the circulation in the tank that ensues.

The experiment was lit from the side using a vertically aligned arrangement of two 300 W Cermax xenon arc lamps fitted with parabolic dichroic reflectors which produced a pair of well-collimated (and relatively cool) beams. The side of the experimental tank was masked off allowing only a thin ($\sim$1 mm) light sheet to pass through the centre of the tank. The plume fluid was marked with fluorescein dye as a passive tracer (see Wong, Griffiths & Hughes 2001 for a more detailed discussion). Video sequences of the experiment were obtained at 24 frames per second using a JAI CVM4+CL digital video camera and were recorded directly to hard disk for subsequent post-processing using DigiFlow (Dalziel 2006). An image of a grid of known mesh size was captured allowing real-world measurements to be taken from the digital video.

The flow rate was measured using two rotameters (Omega FLR1007 series) accurate to $\pm 2\%$ over the maximum range of the flow meter. For the present experiments the errors are of the order of 1% corresponding to an error in the measured volume flux of approximately $2 \times 10^{-8}\,\mathrm{m^3\,s^{-1}}$. The densities of the plume and ambient fluid were measured using an oscillating U-tube density meter (Anton Paar DMA 5000). The approximate errors in these density measurements were smaller than 0.01%.

4.2. *Experimental technique and analysis*

We started an individual experiment by putting the mixing valve in a position such that both header tanks could feed the plume and with the timing light-emitting diodes (LEDs) in the initial configuration. We opened the tap below the nozzle, creating a strong plume within the experimental tank. This plume was allowed to establish itself, typically over times greater than 30 s. We then started the recording process, capturing approximately 10 s of this initial plume. At $t = 0$ we switched the mixing valve so that only one of the two constant-head tanks could feed the nozzle, but the flow rate from that constant-head tank remained unchanged since the pressure drop across the needle valves was much higher than the pressure drop through the nozzle or along the pipes. Switching the mixing valve over caused the flow rate from the other constant-head tank to be quickly reduced to zero (approximately 0.2 s). Switching the mixing valve over also caused the timing LEDs to change over, allowing synchronization of all individual movies to create the ensemble. Approximately 20 s after the mixing valve was switched over we stopped the recording process. It was found that after approximately 8–10 individual experiments the main experimental tank needed to be drained and refilled due to the buildup of tracer.

We took an initial movie of the experimental tank before a plume was created. We time-averaged this movie and thus obtained a good measure of the low-level

† The turbulent plume nozzle was originally conceived by Dr Paul Cooper of the Faculty of Engineering, University of Wollongong, NSW, Australia. A full description can be found in Hunt & Linden (2001).

General experimental values		*Non-dimensional initial and final values*		
Plume nozzle diameter	$\varnothing_\star = 2.9 \times 10^{-3}\,\mathrm{m}$	Mass flux	$Q_0 = 11.77$	$Q_1 = 2.40$
Plume fluid density	$\rho_\star(0,t) = 999\,\mathrm{kg\,m^{-3}}$	Momentum flux	$M_0 = 15.23$	$M_1 = 0.64$
Ambient fluid density	$\rho_{\infty\star} = 1180\,\mathrm{kg\,m^{-3}}$	Buoyancy flux	$F_0 = 1.00$	$F_1 = 0.20$
Mixing valve turnover	$t_{a\star} = 0.208\,\mathrm{s}$	Laziness	$\Gamma_0 = 0.19$	$\Gamma_1 = 4.57$
		Reynolds number	$\mathscr{R}_0 = 858$	$\mathscr{R}_1 = 175$

Dimensional experimental values		
Mass flux	$Q_{0\star} = 2.312 \times 10^{-3}\,\mathrm{kg\,s^{-1}}$	$Q_{1\star} = 4.721 \times 10^{-4}\,\mathrm{kg\,s^{-1}}$
Momentum flux	$M_{0\star} = 6.838 \times 10^{-4}\,\mathrm{kg\,m\,s^{-2}}$	$M_{1\star} = 2.852 \times 10^{-5}\,\mathrm{kg\,m\,s^{-2}}$
Buoyancy flux	$F_{0\star} = 3.540 \times 10^{-3}\,\mathrm{kg\,m\,s^{-3}}$	$F_{1\star} = 7.228 \times 10^{-4}\,\mathrm{kg\,m\,s^{-3}}$

TABLE 1. The experimental values used in the experiments of § 5.1 and § 5.2. A subscript 0 indicates the initial value and a subscript 1 denotes the final value after the mixing valve has been switched over.

background light intensity. We subtracted this averaged image from all the experimental movies captured. The exact distribution of the light-sheet intensity created by the two arc lamps was extremely difficult to measure *a priori*. Therefore, we time-averaged the initial centreline light intensity of the ensemble 'steady plume' over the first 10 s before the mixing valve was switched over. We then divided this time-average by the theoretical prediction for the steady tracer distribution of the passive tracer ($c \propto g'$), generating a constant time-independent one-dimensional data array. We then divided all the individual experimental images by this scaled data array to remove the (unknown) effect of the light-sheet spatial variation. This scaled data array is the only 'tuning parameter'. Where we have removed small-scale noise it has been carried out using a low-pass filter in the spatial and temporal directions with cutoff scales 0.02 m and 0.85 s, respectively.

5. Experimental analysis

We begin in § 5.1 by discussing the behaviour of an individual realization before discussing in § 5.2 the behaviour of our ensemble comprising 100 nominally identical realizations.

5.1. *An individual realization*

Figure 3 shows a single realization at three separate times. The experimental values are shown in table 1. Figure 3(*a*) shows the initial statistically steady forced plume. The plume has a high Reynolds number ($\mathscr{R} = 858$ at the source), and is well described by the steady plume theory of Morton *et al.* (1956). This image was taken 4.08 s before the mixing valve was switched over. Figure 3(*b*) shows the plume 4.17 s after the mixing valve has been switched over. Switching the mixing valve over reduces all three of the driving source fluxes and changes the plume from being forced, with laziness parameter $\Gamma = 0.19$, to being lazy with $\Gamma = 4.57$ (where a value of α is required for non-dimensionalization or otherwise we employ the commonly used value of the entrainment constant for plumes, $\alpha = 0.083$). This reduction in source strength causes a narrowing section to propagate up the plume and can be seen in figure 3(*b*), indicated on the right-hand side of image, with the narrowest section at approximately $z_\star = 0.23$ m. During these experiments the plume remained connected together as a single plume at all times. Figure 3(*c*) shows the re-established steady plume, now with weaker source conditions.

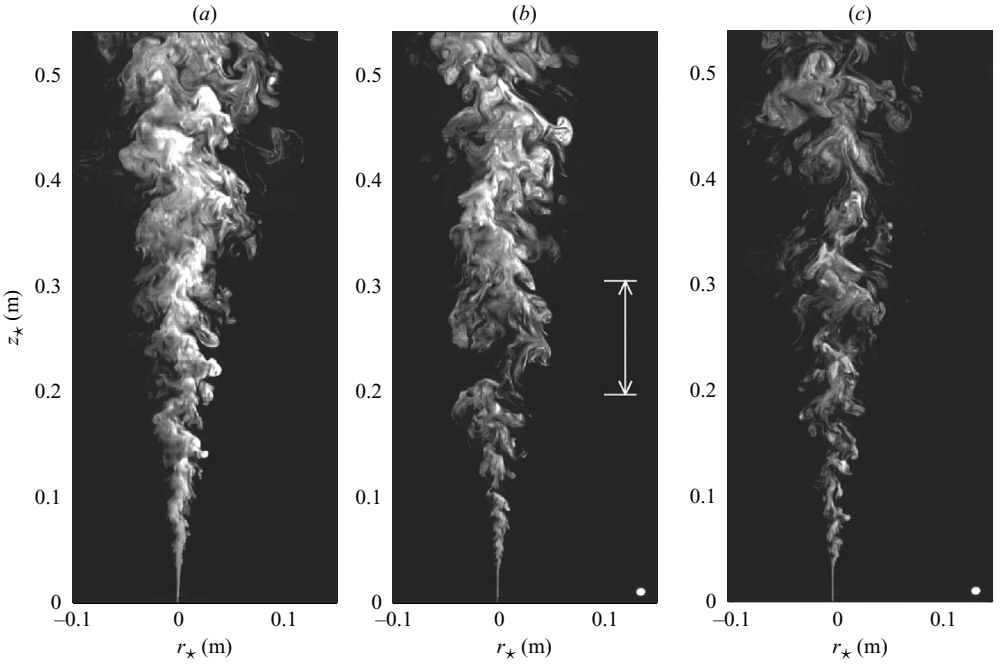

FIGURE 3. Individual realizations of: (*a*) the initial established steady strong plume at $t_\star = -4.08$ s; (*b*) the plume showing a transient necking region (*b*) at $t_\star = 4.17$ s; and (*c*) the newly established weaker plume at $t_\star = 16.33$ s. The small white circle in the bottom right of (*b*) and (*c*) is the (upper) timing LED used to synchronize the experiments. Part (*b*) shows that a transient signal passes up the plume (indicated on the right of the image), causing the plume width to narrow (near $z_\star \approx 0.23$ m), but does not allow the plume to pinch-off into two separate structures. The approximate bounds for the transient region are calculated with (5.1*a–b*).

In figure 3(*b*, *c*) (and later in figure 4), a small region extending from $z_\star = 0$ m to $z_\star = 0.025$ m exists, where the expected conical shape of the plume is not observed. This is due to the low final Reynolds number at the nozzle, employed to try to make pinch-off as likely as possible. However, as was shown in § 3, this small region near the nozzle, far removed from the transitional region, can be accounted for by a virtual origin correction if desired. Use of a virtual origin correction in no way changes our prediction that the transitional region will realize a $b = z/3$ profile and so for simplicity we have not done so.

5.2. *An ensemble of realizations*

Figure 4 shows images averaged across our ensemble of 100 nominally identical experiments at times corresponding to the images shown in figure 3. As the mixing valve is switched over in a given experiment, the timing LEDs change, from a lower LED (not visible in the images of figures 3 and 4 due to cropping) being on and an upper LED being off to a lower LED being off and an upper LED being on (shown in figures 3*b*, *c* and 4*b*, *c*). The intermediate time, as the valve is being switched over, during which both LEDs are briefly off ($\sim$0.04 s) is used to synchronize the individual movies in order to make the ensemble. The images shown have not been filtered, but the unknown spatial distribution of the light sheet has been scaled out using the technique described above in § 4.2.

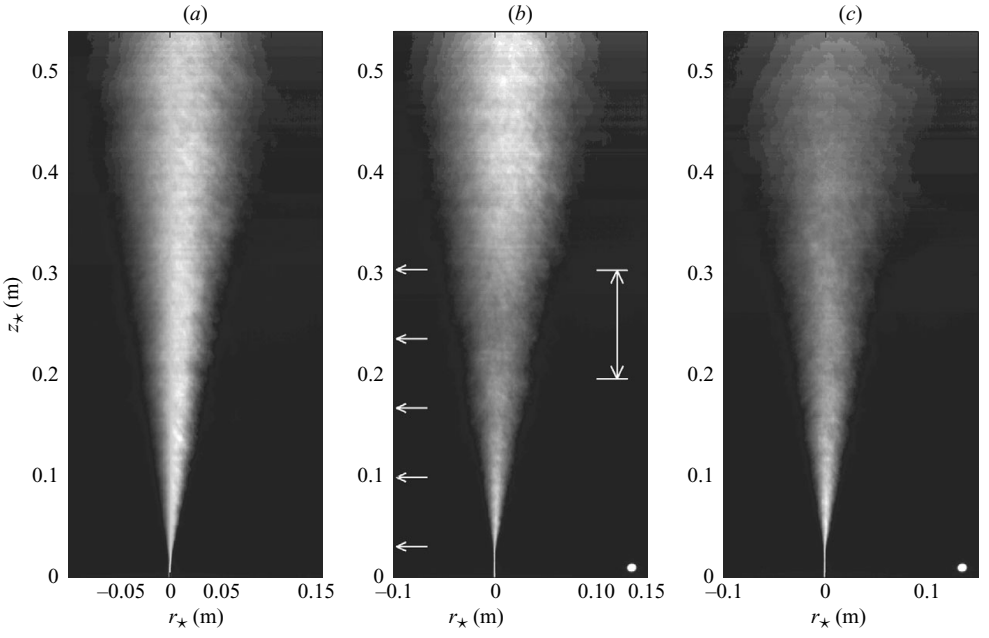

FIGURE 4. Ensemble realizations of: (*a*) the initial established steady strong plume at $t_\star = -4.08$ s; (*b*) the plume showing a transient necking region at $t_\star = 4.17$ s; and (*c*) the newly established weaker plume at $t_\star = 16.33$ s. The small white circle in the bottom right of (*b*) and (*c*) is the (upper) timing LED used to synchronize the experiments. Part (*b*) shows that a transient signal (indicated as in figure 3*b*) passes up the plume, causing the plume width to narrow, but does not allow the plume to pinch off into two separate structures. The white arrows in the left of (*b*) correspond to the heights used in figure 5.

Figure 4(*a*) shows the ensemble of all the experimental plumes at a time $t_\star = -4.08$ s, before the mixing valve is switched over. This is an ensemble of the strong initial forced plumes. Figure 4(*b*) shows the ensemble over the individual experiments at a time $t_\star = 4.17$ s, after the mixing valve has been switched over. The darker region at $0.2\,\mathrm{m} \lesssim z_\star \lesssim 0.3\,\mathrm{m}$ is the transient signal propagating up the plume. Interpreted as a top-hat radius (see § 5.3), this darker region corresponds to the predicted narrowing of the plume radius. Figure 4(*c*) corresponds to the ensemble over the individual experiments at a time $t_\star = 16.33$ s, well after the mixing valve has been switched over. This is now effectively a new statistically steady plume based on the new weaker source conditions. It can be seen that the overall concentration of passive tracer is less than that in the initial plume shown in figure 4(*a*).

5.3. *Analysis of the ensemble*

Figure 5 demonstrates that the modelling assumption of self-similarity in the cross-plume profiles throughout a plume undergoing temporal changes is valid. This self-similarity was simply assumed in the derivation of the model equations (2.4) in S06*b*, but is strongly supported by this new experimental evidence. As can be seen in figure 5, the normalized passive tracer concentration remains approximately Gaussian across the transient narrowing region that propagates up the plume. The specific image used for this calculation is figure 4(*b*). The Gaussian radius b and concentration maximum $c_{m\star}$ were calculated by taking logarithms of the concentration

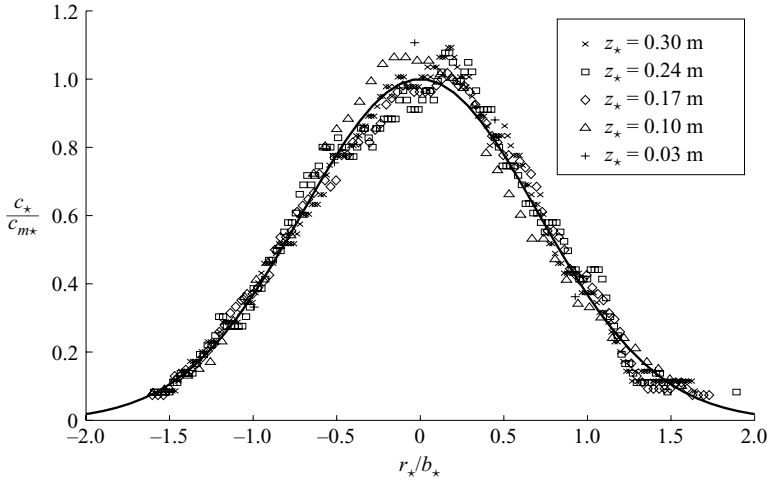

FIGURE 5. The plume maintains a self-similar approximately Gaussian tracer profile throughout the transient region. The data points correspond to the normalized tracer distribution at five different heights of the central image of figure 4. The solid black line shows the Gaussian curve $\exp\{-r^2\}$.

field at a given height and best fitting a quadratic. The five equally spaced heights chosen correspond to a height high up the plume ($z_\star = 0.30$ m) which little information about the source changes has reached, a height low down the plume ($z_\star = 0.03$ m) at which a new steady plume has begun to establish itself with the new steady source conditions, and three intermediate heights through the transient region. All five chosen heights are indicated by white arrows in figure 4(*b*).

For comparison with our theory, we need to recast the approximately Gaussian observed plume profiles in our top-hat framework. This is achieved by first adjusting for the light sheet in our concentration data and then calculating the amplitude, $a(z)$, and the standard deviation, $\sigma(z)$, of the observed Gaussian profile, so that the experimental concentration field is well approximated by $a(z)\exp\{-[r/\sigma(z)]^2/2\}$. For a steady plume, adjusting for the light sheet would mean that $a(z) = 1$. The best-fit Gaussian was found by taking the logarithm of the profile and best fitting a quadratic curve. The total concentration at a given height is therefore given by $c_T(z) = \sqrt{2\pi}a(z)\sigma(z)$. Since the equivalent top-hat radius must have amplitude 1 everywhere by definition, the top-hat radius is given by $b(z) = c_T(z)/1 = \sqrt{2\pi}a(z)\sigma(z)$.

Figure 6 shows the initial and transient interpreted top-hat plume radii corresponding to figure 4(*a*, *b*). The classical steady plume profile of Morton *et al.* (1956) is shown as the dashed line, while the narrower profile predicted by the solutions in (3.1) is shown as the dot-dashed line. The initial plume profile is shown as the thin solid line and agrees well with the classical solution of Morton *et al.* (1956). The thick solid line is the plume $t_\star = 4.17$ s, after the source conditions have been weakened and shows the narrower transient region propagating up the plume. The minimum plume radius is well modelled by the solution predicted in (3.1). In particular we note that the plume does not pinch-off into separate rising thermals.

The plot shown in figure 7 shows the evolution of the passive tracer field at three separate times corresponding to the images in figures 3 and 4. The field $c^{-3/5}$ has

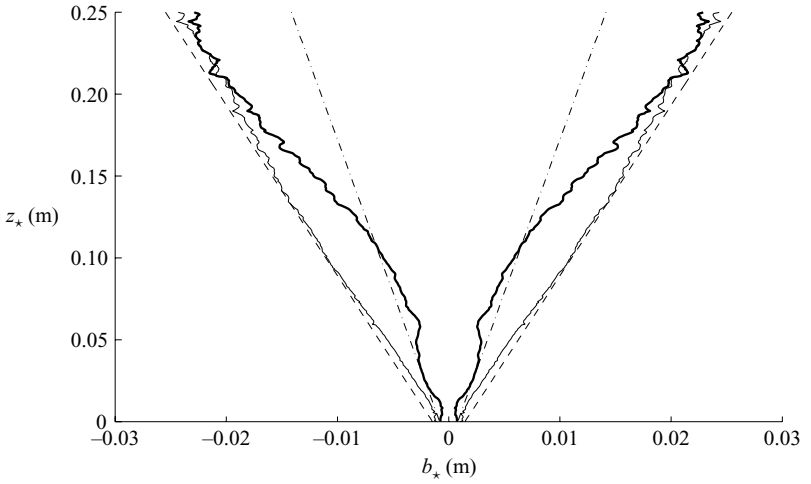

FIGURE 6. A plot of the interpreted top-hat plume radius from figure 4(*b*). The dashed line shows the Morton *et al.* (1956) steady plume profile, and the narrower dot-dashed line shows the predicted minimum plume width as given by (3.1). The thin solid line shows the initial forced plume profile, and the thick solid line shows the plume profile with the transient narrowing region at time $t_\star = 4.17$ s.

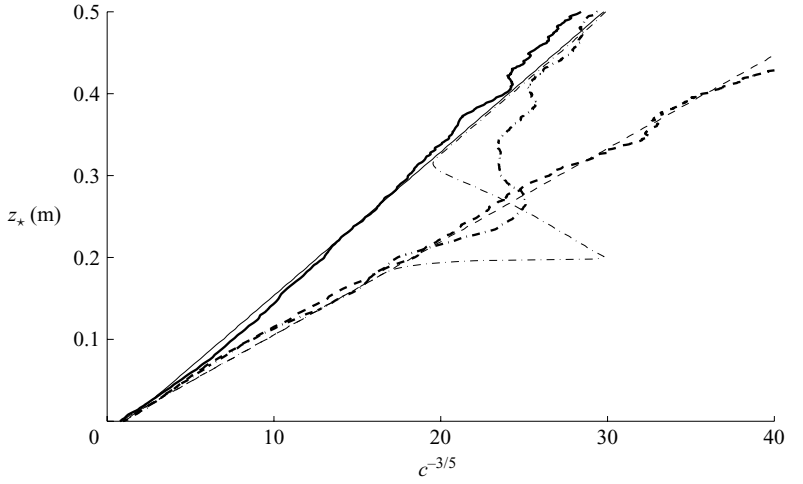

FIGURE 7. A plot of the temporal evolution of the passive tracer concentration. The thin lines are theoretical predictions based on solution of the system (2.4) together with the passive tracer equation (3.3). The thin solid line shows the initial steady distribution of passive tracer, the dashed line shows the final steady distribution of passive tracer. The dot-dashed line shows the passive tracer with the transient signal propagating through it. The thick lines are the equivalent experimental values: the solid line corresponds to $t_\star = -4.08$ s (i.e. figures 3*a* and 4*a*), the dashed line corresponds to $t_\star = 16.33$ s (i.e. figures 3*c* and 4*c*), and the dot-dashed line corresponds to the intermediate time $t_\star = 4.17$ s (i.e. figures 3*b* and 4*b*). The experimental values have been scaled using the technique described in § 4.2 to remove the effect of spatial variation in the light sheet, and have also been spatially and temporally filtered to remove small scale noise.

been plotted so that all curves pass through $(1, 0)$ and the theoretical distribution of passive tracer from a pure plume would appear as a straight line with non-dimensional gradient $\mathrm{d}\left(c^{-3/5}\right)/\mathrm{d}z = 3/(5b_0)$.

The thin lines show the theoretical predictions of the evolution of the passive tracer based on solutions of the governing system of equations (2.4) and the passive tracer evolution equation (3.3). The thin solid line shows the predicted initial distribution of passive tracer, the thin dashed line shows the predicted final distribution and the thin dot-dashed line shows the predicted distribution at the intermediate time, $t_\star = 4.17$ s, after the source conditions have been changed. The thick lines are the experimental measurements. As described in § 4.2, the experimental data have been filtered and the unknown strength of the light sheet has been removed based on the expected initial distribution of the passive tracer.

Figure 7 shows that there is good agreement between the theoretical predictions for the initial and final distributions of the passive tracer. The experimentally measured transient distribution (shown with a dot-dashed line) shows good qualitative agreement with the theoretical prediction. The concentration of passive tracer at the upper section of the plume remains unaffected by the change in source conditions. The lower section of the plume has a concentration extremely close to the final concentration. In the transient region we observe that the concentration of the passive tracer does decrease to a value below that of the final distribution, although the exact position of the top and bottom of the transient region is not as well predicted. It is unsurprising that some sharpness is inevitably lost, compared to the model, in the processes of scaling, filtering and combining to form ensembles, and the fact that the plume contains eddies with some vertical extent which are not captured by the integral top-hat modelling of S06*b*. This vertical extent of the eddies means that some vertical homogenization is observed, due to their overturning and mixing, accounting for an underprediction in the minimum concentration observed within the transitional region.

Figure 8 shows contours of constant-passive tracer concentration in the plume against time. As in figure 7, the model predicts well the concentration of passive tracer before and after the mixing valve has been switched over at $t_\star = 0$ s. The region in which the transient signal propagates up the plume is also well predicted. As derived in S06*b*, the upper limit of the intermediate transient adjustment region is at

$$z_{0\star} = \left(\frac{10}{9\alpha}\right)^{1/2} \left(\frac{F_{0\star}}{\pi\rho_{\infty\star}}\right)^{1/4} t_\star^{3/4}, \tag{5.1a}$$

while the lower limit is at

$$z_{1\star} = \left(\frac{10}{9\alpha}\right)^{1/2} \left(\frac{F_{1\star}}{\pi\rho_{\infty\star}}\right)^{1/4} (t_\star - t_{a\star})^{3/4}, \tag{5.1b}$$

where $t_{a\star}$ is the dimensional turnover time of the mixing valve. The limits, $z_{0\star}$ and $z_{1\star}$ are plotted on figure 8 as dot-dashed lines. The mixing valve turnover time $t_{a\star}$ (listed in table 1) was calculated by measuring the light intensity from both the LEDs in the ensembled experiment. As the mixing valve was switched over the light intensity associated with the LEDs dropped to zero as both LEDs were briefly off, and then the light intensity increased again as the valve was moved into its final position. The time $t_{a\star}$ corresponds to the length of time during which the light intensity associated with the LEDs was varying significantly.

There is also good qualitative agreement in the features of the concentration field in the transient region. As in figure 7, the experiments do not show the sharp changes that the theoretical curves do, partially as a result of the ensemble averaging and filtering.

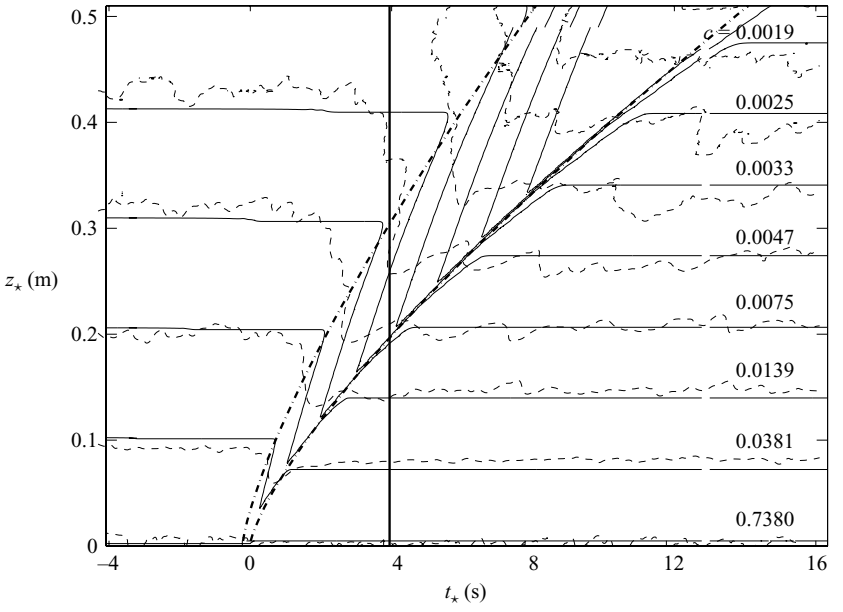

FIGURE 8. A contour plot of lines of constant passive-tracer concentration, as labelled. The solid lines are calculated from the governing system of equations (2.4) together with the passive-tracer equation (3.3). The dashed lines are experimental and have been filtered using the method described in § 4.2.

6. Conclusions

We have presented here, for the first time, experimental evidence of the behaviour of plumes with time-dependent buoyancy flux, which strongly supports the theoretical predictions made in S06*b* and S06*a*. The modelling and experiments were originally motivated by the results of Hunt *et al.* (2003) and a desire to discover whether established plumes could be made to pinch off into individual thermals by reducing their driving-source buoyancy flux. Both our theoretical model and the experiments presented herein indicate that, provided the source strength maintains a turbulent plume throughout the changes in source conditions, and hence the entrainment assumption is valid, an established plume does not break up by a reduction in its source strength alone.

The theoretical model predicted that not only does the plume not pinch off, but it narrows to a non-dimensional width given by $z/3$, or dimensionally $2\alpha z_\star/3$ (where α is the entrainment constant), from its original steady width of $3z/5$, or dimensionally $6\alpha z_\star/5$. Further theoretical investigation has shown that the separable solutions to the governing equations present in S06*b* can be observed with general boundary conditions, provided, as before, that the driving buoyancy flux is sufficiently reduced. Our experiments indicate that a narrowing of the plume radius to $z/3$ is indeed a reasonable prediction. In the present paper we have also introduced a fourth equation to the governing system (2.4) which describes the evolution of a passive tracer within the plume. We have good agreement between the model predictions of the passive-tracer evolution and our experimental observations, particularly outside the transient region. Inside this transient region we observe good qualitative agreement, but the sharp changes in concentration predicted by the model were not observed as clearly, probably due to the necessity of using ensemble averages.

Finally we note that the theoretical predictions of S06*a*, namely that a plume rising through a uniform stratification with buoyancy frequency $N_\star$, which is subject to a reduction in its source strength, stalls in a time $t_\star = \pi/N_\star$, has not been tested herein. However, preliminary results published in Scase *et al.* (2006*c*) indicate that this is again a reasonable prediction, lending further credence to the belief that the predicted time-dependent behaviour of solutions to the governing equations derived in S06*a* are physically realizable.

In conclusion therefore, we find that plumes are remarkably robust and we speculate that only in quite extreme (but still realizable and practical) conditions do they break down into separate puffs.

The authors would like to express their very great gratitude to Professor J. C. R. Hunt for motivating this research and for many useful discussions throughout. We would also like to thank Messrs D. Page-Croft, T. Parkin, R. Raincock and J. Milton, the laboratory technicians at DAMTP, for the manufacture of the key components of the experiments. M.M.S. was funded by NERC award NER/A/S/2002/00892 and by the US-UK Fulbright Commission.

Appendix. Virtual-origin correction for forced plumes

Following Hunt & Kaye (2001), we present a new asymptotic expression for the virtual-origin correction for a forced plume with laziness parameter $\Gamma < 1/2$. For a given plume with unbalanced, non-ideal, source conditions it has been shown (Caulfield 1991; Caulfield & Woods 1995) that in the far field, the plume's properties tend to the power-law solutions of point-source pure plumes. The origin of the point-source pure plume which would match the far field of the non-ideal plume is said to be situated at the 'virtual origin'. Hunt & Kaye (2001) carefully examined the location of the virtual origin for plumes that had steady source conditions which obey $\Gamma > 1/2$. In the present investigation we wish to discuss the virtual-origin correction not only for lazy plumes with $\Gamma \gg 1$, but also for strongly forced plumes with $\Gamma \ll 1$, in particular $\Gamma < 1/2$, a problem first considered by Morton (1959).

We proceed as in Hunt & Kaye (2001) by considering the steady form (2.4). We define normalized non-dimensional quantities q and m such that $Q = Q_0\, q$ and $M = M_0\, m$. It follows from (2.4*a*) and (2.4*b*) that

$$m^{1/2} = \{(q^2 - 1)\Gamma + 1\}^{1/5} \tag{A 1}$$

(see Hunt & Kaye 2001, (24)). Hence, it follows from (2.4*a*) that

$$\frac{z}{b_0} = \int_1^q \frac{1}{\{(\tilde{q}^2 - 1)\Gamma + 1\}^{1/5}} \mathrm{d}\tilde{q}. \tag{A 2}$$

The expression in (A 2) can be rewritten as the following differential equation:

$$q^2 \left(q^2 - \frac{\Gamma - 1}{\Gamma}\right) \frac{\mathrm{d}^2 z}{\mathrm{d}q^2} + \frac{2q^3}{5} \frac{\mathrm{d}z}{\mathrm{d}q} = 0, \tag{A 3}$$

together with the boundary conditions $z(1) = 0$, $\mathrm{d}z(1)/\mathrm{d}q = b_0$. The differential equation in (A 3), together with the boundary conditions, is satisfied by

$$\frac{z}{b_0} = \frac{q}{(1-\Gamma)^{1/5}} \left\{ {}_2F_1\left[\tfrac{1}{5}, \tfrac{1}{2}; \tfrac{3}{2}\right] \left(\frac{q^2\Gamma}{\Gamma - 1}\right) - {}_2F_1\left[\tfrac{1}{5}, \tfrac{1}{2}; \tfrac{3}{2}\right] \left(\frac{\Gamma}{\Gamma - 1}\right) \right\}, \tag{A 4}$$

where ${}_2F_1$ is the hypergeometric function. Using the asymptotic properties of the hypergeometric function expanded about $q \to \infty$ with Γ fixed for the upper limit, and $\Gamma \to 0$ (since $0 < \Gamma < 1/2$) for the lower limit, it follows that

$$\frac{z}{b_0} = \frac{5}{3}\frac{q^{3/5}}{\Gamma^{1/5}} + O(q^{-2/5}) + \frac{\boldsymbol{\Gamma}(-3/10)\,\boldsymbol{\Gamma}(3/2)}{\boldsymbol{\Gamma}(1/5)}\frac{(1-\Gamma)^{3/10}}{\Gamma^{1/2}} - \frac{1}{(1-\Gamma)^{1/5}}\sum_{n=0}^{\infty}\left[\prod_{k=0}^{n-1}(1+5k)\right]\frac{(-1)^n}{5^n\,(1+2n)\,n!}\left(\frac{\Gamma}{1-\Gamma}\right)^n, \quad \text{(A 5)}$$

where care must be taken not to confuse the laziness parameter Γ (defined in (2.5)) with the Gamma function $\boldsymbol{\Gamma}(x)$. The non-dimensional virtual origin correction is therefore given by

$$\frac{z_{vs}}{b_0} = -\frac{\boldsymbol{\Gamma}(-3/10)\,\boldsymbol{\Gamma}(3/2)}{\boldsymbol{\Gamma}(1/5)}\frac{(1-\Gamma)^{3/10}}{\Gamma^{1/2}} + \frac{1}{(1-\Gamma)^{1/5}}\sum_{n=0}^{\infty}\left[\prod_{k=0}^{n-1}(1+5k)\right]\frac{(-1)^n}{5^n\,(1+2n)\,n!}\left(\frac{\Gamma}{1-\Gamma}\right)^n \quad \text{(A 6)}$$

(cf. Hunt & Kaye 2001, (35)). To recover the dimensional virtual-origin correction the non-dimensional virtual-origin correction must be multiplied by $z_\ell = b_{0\star}/(2\alpha b_0)$.

It can be seen from the first few terms of the expansion for z_{vs} given by

$$\frac{z_{vs}}{b_0} \sim \frac{10}{3}\frac{\Gamma(7/10)\Gamma(3/2)}{\Gamma(1/5)}\Gamma^{-1/2} + 1 - \frac{\Gamma(7/10)\Gamma(3/2)}{\Gamma(1/5)}\Gamma^{1/2} + \frac{1}{5}\Gamma + O(\Gamma^{3/2}), \quad \text{(A 7)}$$

that as $\Gamma \to 0$, the virtual-origin correction $z_{vs} \to \infty$. This is as expected since in the limit $\Gamma \to 0$, we have a pure jet, which exhibits different power-law behaviour to a pure plume and so no virtual origin correction can be applied. The first term of expansion (A 7) was given approximately in Morton (1959) (see his (7b)). The numerical value given by Morton, 1.057, is the coefficient of the first term of the present expansion (A 7) multiplied by $2^{3/2}5^{-1/2}$ to account for the different choices in non-dimensionalization, plume profile and definitions of Q, M and F.

REFERENCES

Baines, W. D. & Turner, J. S. 1969 Turbulent and buoyant convection from a source in a confined region. *J. Fluid Mech.* **37**, 51–80.

Batchelor, G. K. 1954 Heat convection and buoyancy effects in fluids. *Q. J. R. Met. Soc.* **80**, 339–358.

Carazzo, G., Kaminski, E. & Tait, S. 2006 The route to self-similarity in turbulent jets and plumes. *J. Fluid Mech.* **547**, 137–148.

Caulfield, C. P. 1991 Stratification and buoyancy in geophysical flows. PhD Thesis, University of Cambridge, UK.

Caulfield, C. P. & Woods, A. W. 1995 Plumes with non-monotonic mixing behaviour. *Geophys. Astrophys. Fluid Dyn.* **79**, 173–199.

Caulfield, C. P. & Woods, A. W. 1998 Turbulent gravitational convection from a point source in a non-uniformly stratified environment. *J. Fluid Mech.* **360**, 229–248.

Dalziel, S. B. 2006 DL Research Partners, http://www.damtp.cam.ac.uk/lab/digiflow

Hunt, G. R. & Kaye, N. B. 2001 Virtual origin correction for lazy turbulent plumes. *J. Fluid Mech.* **435**, 377–396.

Hunt, G. R. & Linden, P. F. 2001 Steady-state flows in an enclosure ventilated by buoyancy forces assisted by wind. *J. Fluid Mech.* **426**, 355–386.

Hunt, J. C. R., Vrieling, A. J., Nieuwstadt, F. T. M. & Fernando, H. J. S. 2003 The influence of the lower boundary on eddy motion in convection. *J. Fluid Mech.* **491**, 183–205.

Kaminski, E., Tait, S. & Carazzo, G. 2005 Turbulent entrainment in jets with arbitrary buoyancy. *J. Fluid Mech.* **526**, 361–376.

Morton, B. R. 1959 Forced plumes. *J. Fluid Mech.* **5**, 151–163.

Morton, B. R., Taylor, G. I. & Turner, J. S. 1956 Turbulent gravitational convection from maintained and instantaneous sources. *Proc. R. Soc. Lond.* A **234**, 1–32.

Scase, M. M., Caulfield, C. P. & Dalziel, S. B. 2006*a* Boussinesq plumes with decreasing source strengths in stratified environments. *J. Fluid Mech.* **563**, 463–472 (herein referred to as S06*a*.).

Scase, M. M., Caulfield, C. P., Dalziel, S. B. & Hunt, J. C. R. 2006*b* Time-dependent plumes and jets with decreasing source strengths. *J. Fluid Mech.* **563**, 443–461 (herein referred to as S06*b*.).

Scase, M. M., Caulfield, C. P., Dalziel, S. B. & Hunt, J. C. R. 2006*c* Plumes and jets with time-dependent sources in stratified and unstratified environments. In *Proc. 6th Intl Symp. on Stratified Flows* (ed. G. N. Ivey), 112–117.

Scase, M. M., Caulfield, C. P., Linden, P. F. & Dalziel, S. B. 2007 Local implications for self-similar turbulent plume models. *J. Fluid Mech.* **575**, 257–265.

Wong, A. B. D., Griffiths, R. W. & Hughes, G. O. 2001 Shear layers driven by turbulent plumes. *J. Fluid Mech.* **434**, 209–241.

Woods, A. W. 1997 A note on non-Boussinesq plumes in an incompressible stratified environment. *J. Fluid Mech.* **345**, 347–356.